ISSN: 2710-0588

Studies on the Properties of Nitrogen as a Diluent in Laminar Premixed $NH_3/CO/H_2$/air Flames at Elevated Temperature and Pressure

Mengxin Guo, Jun Song*

School of Mechanical and Power Engineering, Henan Polytechnic University, Jiaozuo, China

*Corresponding author E-mail: sj@hpu.edu.cn

Abstract

This study provides a comprehensive investigation of the laminar flame propagation characteristics of $NH_3/N_2/CO/H_2$/air mixtures under high-temperature and high-pressure conditions across a wide range of equivalence ratios. Laminar burning velocities (LBVs) were determined using the spherical flame propagation method, which enables accurate evaluation of intrinsic flame properties while minimizing the influence of external disturbances. Particular emphasis was placed on the effects of equivalence ratio and N_2 dilution volume fraction, both of which exert significant influences on flame dynamics.The results reveal that LBV decreases monotonically with increasing N_2 dilution, while it increases with elevated initial temperature. In contrast, the dependence of LBV on equivalence ratio exhibits a non-monotonic behavior, reflecting the complex interplay among heat release, transport phenomena, and flame structure. As an inert diluent, N_2 significantly suppresses flame propagation by reducing the net reaction rate of critical chain-branching reactions, altering the ammonia consumption pathway, and ultimately lowering NOX formation. The presence of N_2 not only affects flame stability but also modifies the emission characteristics of ammonia-based fuel mixtures.Overall, these findings provide new insights into the combustion performance of $NH_3/N_2/CO/H_2$/air mixtures and demonstrate that the use of N_2 as a diluent can effectively reduce NOX emissions, thereby offering valuable guidance for the design and optimization of cleaner, ammonia-fueled energy systems.

Keywords

Ammonia, Diluent, Laminar Burning Velocity, Flame Instability.

1. Introduction

Since the 20th century, the problem of environmental pollution has become increasingly serious. In response to the national call to reduce carbon dioxide emissions, promoting the development of carbon-free renewable energy sources is imperative in order to slow the rise of environmental pollution [1]. Ammonia (NH_3) has garnered significant attention [2]; But using it as fuel presents a number of difficulties. Ammonia has a lower LBV than traditional hydrocarbon fuels, peaking at around 7 cm/s [3]. Ammonia has a very high minimum ignition energy. From a chemical point of view, ammonia is composed of N-H bonds, and the dissociation of N-H bonds requires higher energy, that is, higher ignition energy is required. Compared to traditional hydrocarbon fuels, ammonia fuel requires an ignition energy that is around an order of magnitude higher [4]. Therefore, a high-energy igniting mechanism is required when using ammonia as fuel in internal combustion engines [5]. Ammonia has a narrower flammable limit and higher NO_x emissions, the formation mechanism of ammonia NO is different from that of hydrocarbon fuel combustion to produce thermal type NO, mainly for the fuel type NO produced in the combustion process, and we need to develop a new NO control method [6].

ISSN: 2710-0588

A zero-carbon fuel with enormous potential for use in industrial boilers, engines with internal combustion, and gas-powered turbines is ammonia. Its limited reactivity and tendency to emit a lot of NO_x, however, pose significant problems. Nitrogen dilution can effectively lower flame temperature, thereby reducing NO_x formation and enhancing combustion stability. In gas turbines, ammonia can be co-fired with hydrogen or natural gas to improve efficiency and mitigate carbon emissions. For internal combustion engines and boilers, ammonia combustion can optimize thermal energy conversion and minimize pollutant emissions [7]. This study investigates ammonia's combustion qualities to potentially aid in the creation of future low-carbon energy systems.

Internal combustion engines' use of ammonia is restricted by the previously listed issues. Numerous ongoing research aim to enhance NH_3's performance in order to improve its combustion status, LBV, and combustion intensity [8].By effectively combining NH_3 with other hydrocarbon fuels, the LBV of the NH_3/air flame is raised, meeting the need for more ignition energy [9]. The dual impact of syngas, which may both efficiently lower carbon dioxide emissions and speed up the flame propagation of ammonia, is particularly noteworthy among these gas mixes. The primary constituents of syngas encompass hydrogen (H_2), carbon monoxide (CO), and methane (CH_4), alongside significant quantities of diluent gases, including carbon dioxide (CO_2) and nitrogen (N_2). In practical applications, the co-combustion of NH3 with syngas has stronger combustion properties and lower pollution emission potential [10]. However, combustion of a mixture of ammonia and syngas also produces excessive nitrogen oxide (NO_x) emissions. Dilution gas, that is, the incorporation of a certain proportion of gas into the fuel, may improve the mixture's combustion characteristics by altering the fuel and oxidant concentrations as well as the mixture's physicochemical qualities [11].

Some studies have shown [12,13] that mixed gas dilution or exhaust gas recirculation (EGR) technology is extensively employed in compression ignition engines to effectively mitigate NO_x emissions and lower the combustion temperature. EGR mainly reduces the oxygen concentration and flame temperature by introducing part of the exhaust gas after combustion, thereby inhibiting the formation of NO_x; nitrogen dilution reduces the activity of the combustion reaction by directly adding N_2, and simultaneously lowers the flame temperature. These techniques have been demonstrated to be crucial for enhancing internal combustion engines' environmental performance by reducing the amount of nitrogen oxides produced during combustion.

The LBV of NH_3/syngas and air mixes at standard temperature and pressure was examined experimentally by Han et al. [14] using the heat flux method. The LBV of many mixes, such as NH3/syngas/air, NH_3/CO/air, and NH_3/H_2/air, was evaluated by Wang et al. [15] using the heat flux technique at 298 K and 5 atm pressure. Their study involved an in-depth kinetic analysis, focusing on how pressure influences the LBV. Under similar experimental circumstances, Lee et al. [11,16] used the spherical flame expansion technique to study the unstretched LBV and Markstein number of NH3/air premixed flames with hydrogen addition. The results demonstrated that the presence of H_2 considerably increases the combustion velocity of NH_3/air mixtures. However, the study also found that the injection of H_2 raises NO_X and N_2O emissions. Furthermore, when the mixtures were fuel-rich, both NO_X and N_2O emissions were significantly lower compared to fuel-lean conditions. These findings suggest that employing a hydrogen enrichment strategy in NH_3/air mixtures can effectively improve LBV while reducing nitrogen oxide production. After examining NO_X emissions and combustion stability, Mousavi et al. [17,18] came to the conclusion that a larger NH_3 content lowers the concentrations of OH radicals, which consequently increases the ignition delay time. Similarly. Kiani et al. [19] looked at how the equivalency ratio, CO concentration, and NH_3 levels affected the mild combustion characteristics of syngas/NH_3/air mixtures. Their findings, which showed a considerable increase in NO_X generation under fuel-lean conditions, demonstrated the important function

ISSN: 2710-0588

that equivalency ratio plays in controlling pollutant emissions. In addition to analyzing the properties of NO production at different cracking ratios, Mei et al. [20,21] investigated into the LBV trends for $NH_3/H_2/N_2$/air mixes at various cracking ratios and pressures. Compared with the studies by Han et al. and Wang et al., this study adopted different dilution rate ranges, equivalence ratio settings, and experimental conditions, providing more comprehensive nitrogen oxide emission data and more detailed reaction mechanism analysis.

The combustion properties of ammonia-syngas mixtures with different N_2 dilution levels are examined in this work. The aim is to better understand how these diluents affect flame behavior, thereby contributing to the optimization of combustion processes for enhanced performance and reduced emissions in future energy systems. When ammonia is used as a fuel, the N_2 present in NH_3 is a major contributor to NO_X emissions. Since there is a lack of experimental data on the basic properties of these flames, more research is needed to investigate how N_2 dilution affects the combustion performance of NH_3/syngas/air mixes.

This study investigates the properties of flame propagation in NH3/syngas/air mixtures across a range of dilution levels (X = 0–0.3), initial temperatures (T_u = 298K,373 K), initial pressures (P_0 = 1atm, 3 atm), and equivalence ratios (Φ = 0.8–1.4). The study offers a comprehensive analysis of how the equivalence ratio, temperature, and dilution ratio affect the LBV. The study measures the impact of thermal-diffusive and hydrodynamic instabilities on flame behavior using linear stability theory. Additionally, numerical simulations are used to look at how N2 dilution affects LBV chemically and thermally.

2. Experiment and Numerical Simulation

2.1. Experimental Methods

A constant-volume burning chamber, a pressure gauge, a gas distribution system, an igniting system, and a flame photography apparatus make up the experimental setup, which is schematically shown in Figure 1. Inside a 400 mm diameter by 400 mm high stainless steel cylindrical constant-volume combustion chamber, the flame burns and spreads.The gas distribution system consists of an air compressor, a vacuum pump, and cylinders for NH_3, H_2, CO, and N_2. A digital pressure gauge that can withstand high temperatures carefully regulates the intake process. Fuel and oxidizer are added to the combustion chamber with 99% accuracy after it has been emptied prior to the tests. To ensure uniform gas temperature and mixing within the chamber, an agitator is included in the setup. In addition, a K-type thermocouple and a PID thermostat are employed to keep the combustion chamber's temperature uniform. [22].

A focusing lens, an LED light source, a convex lens assembly, two linear stages, two concave mirrors, a high-speed camera (Phantom Miro M310), and a computer are all part of the high-speed Schlieren photography system. With a resolution of 1024 × 768 pixels, the camera's frame rate can vary from 6000 to 10,000 frames per second, depending on how rapidly flames spread. The procedure for acquiring flame images is as follows: Light emitted from the LED source traverses the convex lens assembly and is directed towards one of the concave mirrors. The refracted light beam subsequently passes through a fixed-volume chamber before reaching the second concave mirror, where it is redirected into the focusing lens and ultimately captured by the high-speed camera. This setup enables efficient recording of transient phenomena during the experiment, with the collected flame images being processed and stored via the computer.

A high-energy igniter and two tungsten wire electrodes placed in the middle of the combustion chamber make up the ignition system. To establish a high-temperature experimental environment, the combustion chamber is equipped with an electric heating belt capable of elevating the internal temperature to 373 K. Six K-type thermocouples are also positioned

ISSN: 2710-0588

thoughtfully around the combustion chamber to enable real-time temperature distribution monitoring.

The experimental procedure begins by heating the constant-volume chamber to the target temperature and establishing a vacuum environment through evacuation with a vacuum pump. The beginning pressure, equivalence ratio, and Dalton's law of partial pressures under the specified experimental conditions are then used to determine the partial pressures of each gas. In order to produce the necessary mixture gas, fuel and air are then supplied into the combustion chamber in line with the ratio of partial pressures for each gas. Once filling is completed, a gas stirring device is activated for five minutes to ensure uniformity in gas temperature and mixture. Once homogeneity has been reached, a high-energy igniter is used to light an ignition electrode made of tungsten wire that is situated in the combustion chamber's center. Computer monitoring is used to gather experimental data in real time. Upon completion of data recording, gases inside the combustion chamber are evacuated using a vacuum pump followed by three minutes of air blowing utilizing an air compressor. This step aims to remove residual products generated during combustion and minimize NH_3 adsorption residue that may potentially impact subsequent experimental results.

The main reasons for the equivalency ratio error in this inquiry are the gas partial pressure technique and the accuracy digital pressure gauge. Typically, the inaccuracy falls between 1% and 3%. With an inaccuracy of less than 1%, the starting temperature precision is kept within the ± 3K range. The precision of the beginning pressure is kept within ± 3kPa with an error of less than 3%. Because of the high-speed camera's great resolution, the measurement error is deemed insignificant when extracting the flame radius. Lastly, this study's total experimental error is less than 5%. Considering inherent uncertainties associated with experiments conducted under identical initial conditions, to ensure that the experimental results are precise, each trial must be carried out at least three times. The evaluation of uncertainty for LBV varies from 0.5 to 2.1 cm/s, as shown by error bars, taking into account the measurement uncertainty of thermocouples, which is estimated at 5 K for temperature, and pressure regulated by high-precision pressure transmitters, which has an uncertainty of 1 KPa.

The combustion reaction equation for the $NH_3/CO/H_2/N_2$/air flame combination is defined as follows:

$$\begin{aligned} &xNH_3 + yCO + zH_2 + a(O_2 + 3.76N_2) = x/2N_2 + yCO_2 \\ &+(3x+2z)/2H_2O + 3.76aN_2 \end{aligned} \tag{1}$$

$$a = (3x+2z)/4 + y/2 \tag{2}$$

The following defines the N_2 volume percentage in the fuel mixture:

$$x_i = \frac{V_i}{V_{H_2} + V_{N_2} + V_{NH_3} + V_{CO}} \times 100\% \tag{3}$$

Here, Vi stands for the N_2 volume fraction in the mixed fuel and xi for the volume percentage of component i in the blended fuel.

The experimental setup employed in this investigation is shown in Table 1. With the beginning temperature set at 373 K and the initial pressure set at 3 atm, the research aims to investigate how the concentration of N_2 affects the features of flame propagation under high temperature and pressure settings.

ISSN: 2710-0588

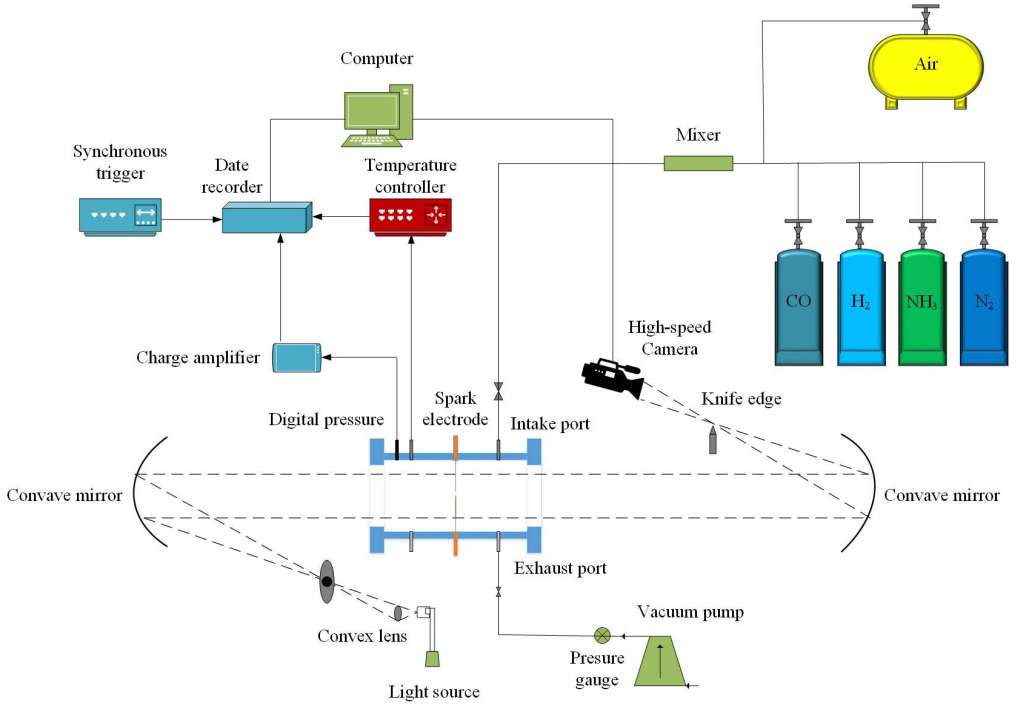

Figure 1. Schematic diagram of the experimental setup.

Table 1. Experimental conditions

Fuel component(vol%)				x_{N2}(%)	Equivalence ratio	Temperature/K	Pressure/atm
NH_3	CO	H_2	N_2				
50	25	25	0	0	0.8,1.0,1.2,1.4	373	3
45	22.5	22.5	10	10	0.8,1.0,1.2,1.4	373	3
40	20	20	20	20	0.8,1.0,1.2,1.4	373	3
35	17.5	17.5	30	30	0.8,1.0,1.2,1.4	373	3
				0-30	1.0	273	1,3

2.2. Data Processing

To produce flame images, a high-speed camera captures the spread of mixed fuel flames. These images were captured using Schlieren technique and a high-speed camera, and the data was processed using computer software. Image-Pro Plus (IPP) software was used in this work to calculate the flame radius (R_f) and the exact location of the flame boundary. Accurate calculation of the LBV depends on the careful selection of the flame radius range. The unstable transition phase that a spherical flame goes through as it moves from the ignition core to the propagation front is responsible for this phenomena. In the early phases of flame creation, the ignition energy has a significant impact on the propagation dynamics. The impact of wall restrictions on flame propagation becomes more noticeable in later phases [23]. The flame propagation mechanism will be further impacted by the cylindrical combustion chamber's border when the flame radius is big [24]. To improve the precision of LBV calculation, extensive research has been devoted to determining an optimal range for the flame radius. This effort aims to refine the parameters critical for accurate LBV assessment, thereby enhancing the reliability of combustion models and analyses [25]. To ensure the exclusion of extraneous variables such as spark ignition, pressure increase, and system limitations, this study meticulously selected a range of flame radii from 5 to 30 mm. This approach facilitates a more controlled experimental environment, thereby enhancing the reliability and validity of the results [26,27]. The LBV based on laminar spherical flame theory was computed using the spherical expanding flame technique [28]. By computing the flame's instantaneous radius from

ISSN: 2710-0588

the image of the spherical spreading flame, the stretched flame velocity S_b is found, which is [29].

$$S_b = \frac{dR_f}{dt} \tag{4}$$

where t represents time while R_f signifies the instantaneous radius of the flame. It is important to note, however, that the spherical propagation of flames can be influenced by aerodynamic strain or curvature-induced stretching effects, which may alter the flame's propagation dynamics. As a result, determining S_b (stretched flame speed) for a given flame becomes contingent upon evaluating its overall stretchability represented by the flame stretching rate (κ)-an indicator denoting how rapidly its surface area changes with respect to time and unit area [30].

$$\kappa = \frac{1}{A} \cdot \frac{dA}{dt} = \frac{2}{R_f} \cdot \frac{dR_f}{dt} = \frac{2}{R_f} \cdot S_b \tag{5}$$

where A is the spherical propagation area of the flame surface.

Numerous relationships between S_b and κ have been proposed in the literature [31], which can eliminate the interference effect of stretching on measuring S_b by projecting S_b to zero stretch, and the propagation velocity of unstretched flame can be obtained by this method S_b^0.

$$S_b = S_b^0 - L_b k \tag{6}$$

where L_b is the Markstein length. The mass conservation of the unstretched flame S_L is used to compute the LBV. [32].

$$\rho_u S_L = \rho_b S_b^0 \tag{7}$$

where ρ_u and ρ_b, as determined by CHEMKIN, are the densities of unburned and burnt gas, respectively.

2.3. Linear Stability Theory

The types of flame instability include thermal diffusive instability, buoyancy instability, and hydrodynamic instability [33]. To more accurately quantify the effects of thermal diffusion instability and hydrodynamic instability [34], three important parameters have been introduced in studies [35]. These parameters are used to define the flame thickness (δ_f), thereby providing a more specific and quantitative basis for analyzing related phenomena:

$$\delta_f = \frac{T_{ad} - T_u}{(dT/dx)_{\max}} \tag{8}$$

where T_{ad} denotes the adiabatic flame temperature, T_u represents the temperature of the unburned mixture, and $(dT/dx)_{max}$ signifies the maximum gradient of the temperature profile. The coefficient of thermal expansion (σ) is calculated by the following formula:

ISSN: 2710-0588

$$\sigma = \rho_u / \rho_b \tag{9}$$

A crucial metric for assessing the degree of heat-mass diffusion imbalance is the Lewis number (*Le*), which is commonly described as:

$$Le = \frac{D_T}{D_M} = \frac{\lambda}{\rho_u C_P D_M} \tag{10}$$

where multicomponent fuel mixtures, the thermal diffusion coefficients and mass diffusion coefficients are denoted as D_T and D_M. C_P stands for the unburned mixture's specific heat capacity at constant pressure. while λ indicates the unburned mixture's heat conductivity. To accurately describe the transport properties in multicomponent fuel mixtures, it is essential to introduce the concept of the effective Lewis number (Le_{eff}), which can be defined through a mathematical expression [36].

$$Le_{eff} = 1 + \frac{(Le_E - 1) + (Le_D - 1)A}{1 + A} \tag{11}$$

where Le_E and Le_D represent the Lewis numbers of reactant excess and reactant deficiency in the mixture, respectively. *A* is the mixing strength, which is obtained from the formula $A = 1 + Ze(\Phi - 1)$, where Φ is the mass ratio of excess to insufficient active agent, and *Ze* is the number of Zel¢dovich.

In addition, the non-dimensionalized perturbation growth rate Σ can be derived by utilizing the formula (12)

$$\sum = \frac{2\pi\sigma}{n}(1 - \frac{2Ma}{Pe})(\omega - \frac{\theta}{Pe}) \tag{12}$$

where *Ma* is the Markstein number. The Markstein can be obtained using Eq:(13) [37]

$$Ma = r_1 + \sigma Ze(Le_{eff} - 1)r_2 / 2 \tag{13}$$

where r_1 and r_2 are calculated like this.

$$r_1 = \frac{\sigma}{\sigma - 1}\int_1^\sigma \frac{\lambda(x)}{x}dx \tag{14}$$

$$r_2 = \frac{1}{\sigma - 1}\int_1^\sigma \frac{\lambda(x)}{x}\ln(\frac{\sigma}{x - 1})dx \tag{15}$$

where *x* represents the dimensionless temperature T/T_u. When ω-Ω/Pe equals zero, the expression for the marginal stability curve can be derived:(16)

ISSN: 2710-0588

$$Pe = \frac{R}{\delta_T} = \frac{\theta(\sigma, Le_{eff}, Pr, n)}{\omega(\sigma, n)} \tag{16}$$

In the above equation, ω and Ω rely on the wave number n, effective Lewis number Le_{eff}, Prandtl number P_r, and coefficient of thermal expansion "σ." The following formula can be used to obtain these coefficients, ω and Ω (17)~(21)

$$\omega = \frac{-(b-a) + \sqrt{(b-a)^2 - 4ac}}{2a} \tag{17}$$

$$a = (\sigma + 1)n + 1 \tag{18}$$

$$b = 2n^2 + (4 + 5\sigma)n + 4 \tag{19}$$

$$c = -(\frac{\sigma - 1}{\sigma})n^3 + 2n^2 + \left[3(\sigma + 1) - \frac{1}{\sigma}\right]n + 2 \tag{20}$$

$$\Omega = \Omega_1 + \frac{Ze(Le_{eff} - 1)}{\sigma - 1}\Omega_2 + \Omega_3 Pr \tag{21}$$

The symbols Ω_1, Ω_2, and Ω_3 indicate the coefficients of heat conduction, molecular diffusion, and viscous diffusion, respectively. See References [37].

Table 2. Detailed information about numerical models

Mechanism name	Species number	Reaction number	Source
Okafor	59	356	[38]
Gri	53	325	[39]
Zhou	21	150	[40]
Mei	40	257	[41]
Han	35	177	[42]

2.4. Numerical Simulation

To have a more profound comprehension of the experimental mechanism analysis, we employed CHEMKIN-Pro software to calculate the one-dimensional free-propagating premixed flame of an NH_3/N_2/syngas/air mixture. The calculation of LBV adopts Okafor-mech [38], Gri-mech [39], Zhou-mech [40], Mei-mech [41], and Han-mech [42]. Table 2 displays the detailed details for each model. Multi-component transport models and thermal diffusion (Soret effect) were taken into account in the simulation. The equivalence ratio was calculated within the range of 0.8 to 1.4. To ensure complete convergence of flame velocity prediction, a starting grid point size of 700 was used for each case, with GRAD set to 0.02 and GRUV set to 0.05.

ISSN: 2710-0588

3. Results and Discussion

3.1. Laminar Burning Velocity of NH_3/N_2/Syngas/Air Mixture

3.1.1. Influence of Diluent N_2 on LBV

Figure 2 compares experimental and simulated results for the LBV of NH_3/N_2/syngas/air mixtures. The LBV demonstrates a non-monotonic trend, through simulation, it was discovered that increasing initially and peaking at Φ = 1.1 before declining as the equivalence ratio rises from 0.8 to 1.4. However, there is a discernible overall decrease in LBV along with a considerable drop in the peak LBV value when the N2 concentration rises from 0 to 0.3. Additionally, the peak shifts to equivalence ratios higher than Φ = 1.1.

As N_2 concentration rises, the inhibitory action of N2 becomes more pronounced, further lowering LBV. Figure 2 presents a comparison between experimentally measured LBVs and simulation results obtained using five different mechanisms. As N_2 content increases, there is an improved agreement between simulation and experimental results. However, variations exist among the simulation results generated by different mechanisms. Three mechanisms (Zhou-Mech, Mei-Mech, and Han-Mech) predict higher LBVs than those observed experimentally, LBV is generally 5-10 points higher. whereas Gri-Mech predicts lower values compared to experimental data.

In contrast, the Okafor mechanism demonstrates better capability in simulating LBVs for NH_3/N_2/syngas/air mixtures across various equivalence ratios and N_2 concentration ranges when compared to other mechanisms as well as experimental findings. Therefore, Okafor mechanism was adopted in the subsequent simulation images.

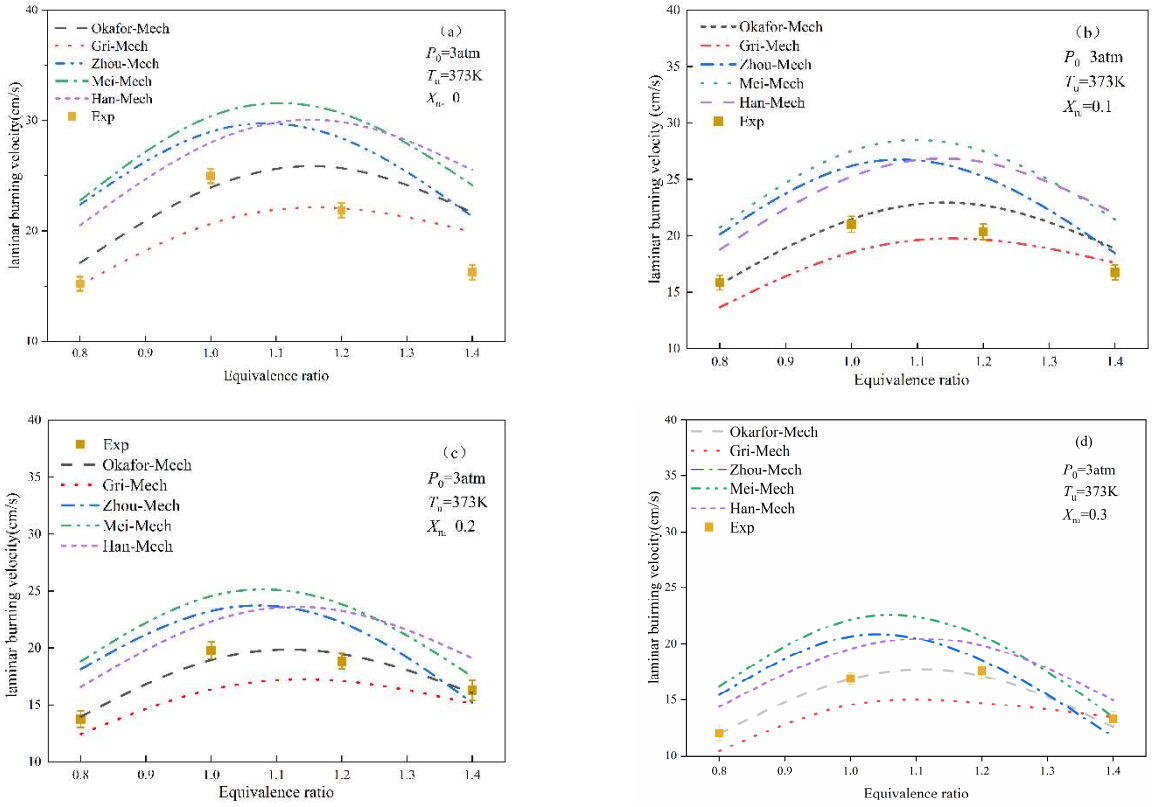

Figure 2. Variation of LBV with equivalence ratio for NH_3/N_2/syngas/air mixtures.

3.1.2. Effects of Starting Temperature and Pressure on LBV

With an equivalency ratio of Φ = 1, Figure 3 shows how the LBV value for the NH_3/N_2/syngas/air mixture varies as the N_2 concentration varies with temperature and

ISSN: 2710-0588

pressure. The experimental conditions include P_0 = 1 atm, T_u = 298 K; P_0 = 3 atm, T_u = 373 K; and P_0 = 3 atm, T_u = 298 K. Figure 3 illustrates the variation in LBV for NH_3/N_2/syngas/air mixture as the N_2 concentration changes under varying temperature and pressure conditions, it is observed that the LBV value exhibits a gradual decrease as the N_2 content increases. Furthermore, a larger LBV value results from a rise in temperature under conditions of constant pressure. These experimental findings align reasonably well with simulation results. A close analysis reveals that at 298 K, 3atm, the LBV value fluctuates between 15 cm/s and 10 cm/s. However, at 373 K, 3atm, the LBV value fluctuates between 25 cm/s and 15 cm/s. Conversely, when keeping temperature constant, variations in pressure have minimal impact on the LBV value. Notably though, experimental data obtained at 3 atm agrees well with simulation results using either Okafor-Mech or Gri-Mech mechanisms. Nevertheless, under atmospheric conditions (1 atm), experimentally determined LBV values are significantly lower than those predicted by simulations. To better understand fluctuations in LBV and enhance agreement between experiments and simulation results, this study examines various equivalence ratios under conditions of P_0 = 3 atm and T_u = 373 K, providing deeper insights into LBV variation trends.

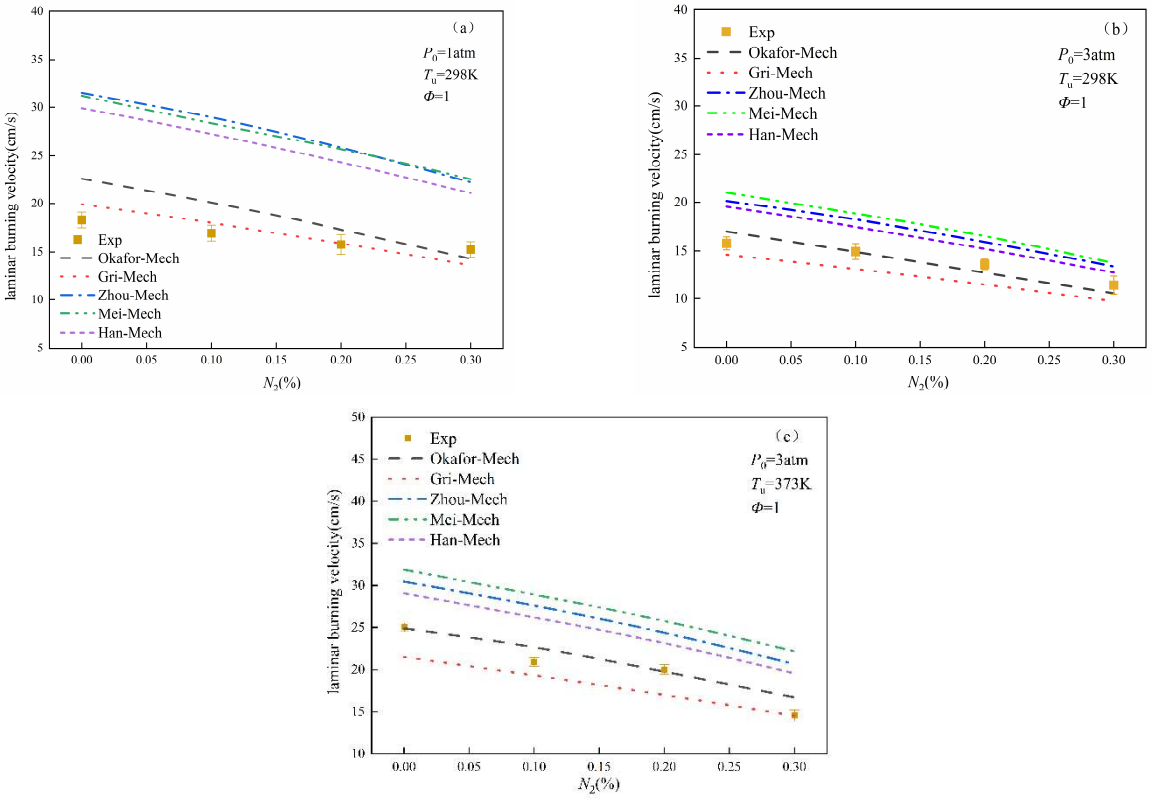

Figure 3. LBV at different temperatures and pressures.

3.2. Flame Instability Analysis

3.2.1. Flame Image Analysis

Figure 4. Flame image of NH3/N2/syngas/air mixture at different equivalence ratios. The experimental conditions were P_0 = 3 atm, T_u = 373 K, and X_n = 0.1. When Φ was set to 0.8, 1.0, 1.2, and 1.4, the premixed flame exhibited a spherical propagation mode that filled the entire chamber. The NH_3/N_2/syngas/air mixture's flame center stayed steady, as the figure makes evident, suggesting that buoyancy had very little effect on flame propagation. Increased flame propagation speeds usually lessen the effect of buoyancy.

ISSN: 2710-0588

In the flame image with N_2 content of 0.1, when Φ = 0.8, the flame surface exhibits a pronounced folding phenomenon, while with the gradual increase of Φ to 1.0, 1.2, and 1.4, the flame surface gradually becomes smoother and the number of cracks decreases. According to the analysis in Figure 6, this is mainly because when P_u = 3 atm, T_0 = 373 K, and Φ = 0.8, Leeff < 1, because of the combined action of the thermal diffusion effect and the hydrodynamic effect, the flame surface exhibits noticeable folds and cracks. As the equivalency ratio increases and Leeff > 1, the influence of diffusive instability steadily diminishes, leading to less folding of the flame surface and a smoother appearance of the flame structure overall.

Figure 5 displays flame propagation images for varying N_2 concentrations at Φ = 1.0. The expansion flame's surface smoothes down and the flame center stays the same as the N_2 concentration increases, indicating less flame instability. At low N_2 concentration, flame instability is more obvious, while at high N_2 concentration, flame instability is weakened. Overall, the increase in N_2 concentration effectively suppresses thermal diffusion instability by reducing local temperature gradients, minimizing local concentration of reaction heat, and altering flame structure. This effect is particularly pronounced during high-temperature combustion, which is beneficial for improving flame stability, especially in the case of complex fuels (such as ammonia and hydrogen mixtures) combustion, where the influence of N_2 is particularly prominent. Next, the specific analysis of flame instability will be further discussed.

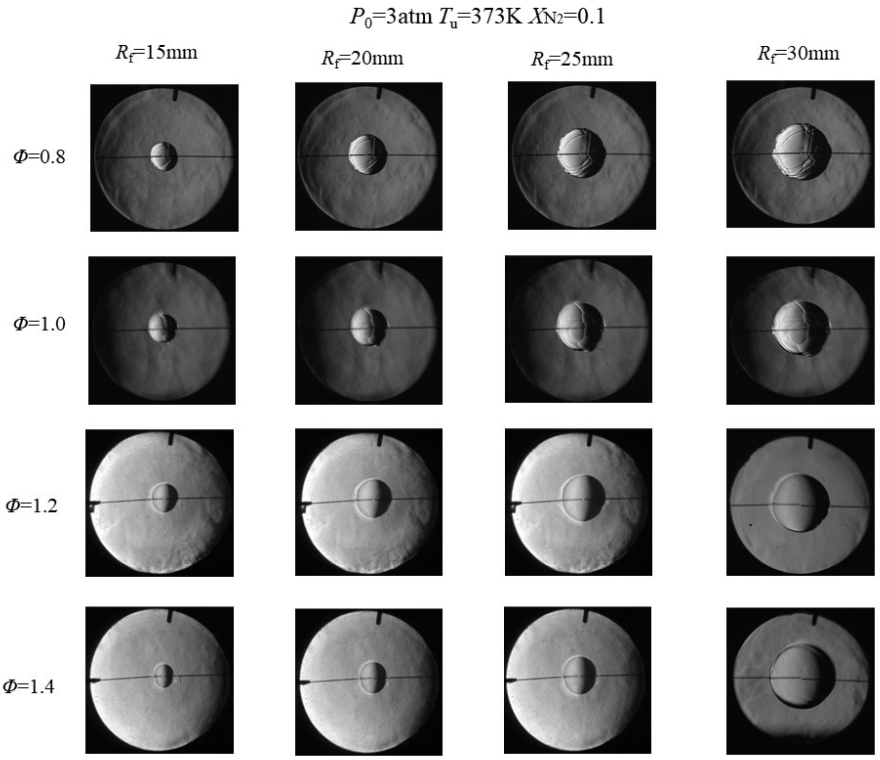

Figure 4. Flame image of NH_3/N_2/syngas/air mixture at different equivalence ratios.

ISSN: 2710-0588

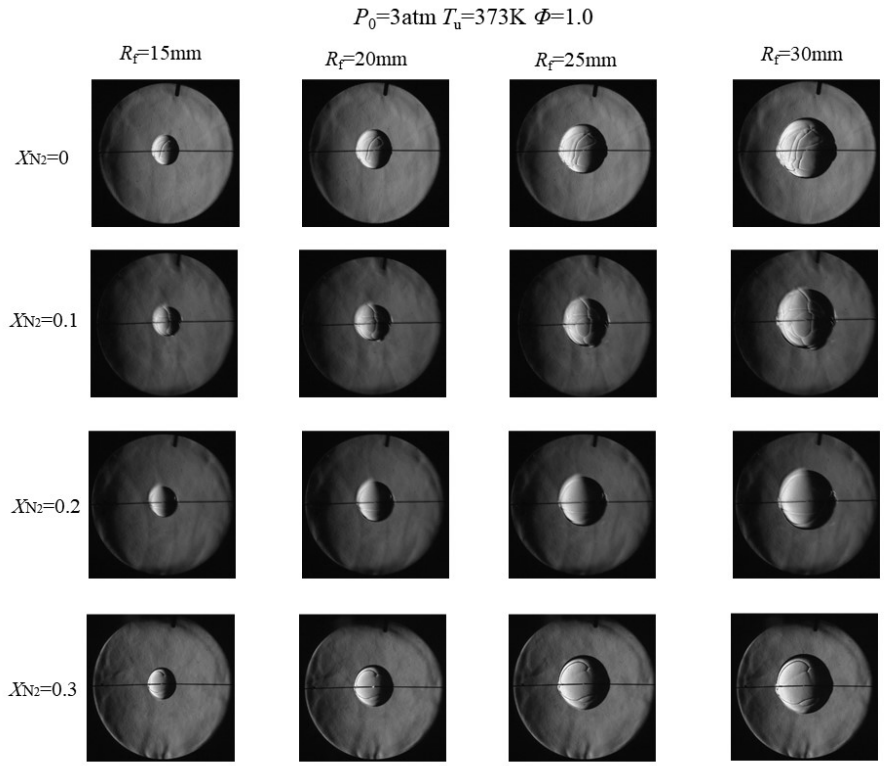

Figure 5. Flame image of NH_3/N_2/syngas/air mixture at different N_2 concentrations.

3.2.2. Effective Lewis Number Analysis

The theory of flame instability states that non-uniform mass diffusion and heat diffusion are the main causes of diffusion instability [43]. The Lewis number (*Le*), which is the ratio of the thermal diffusivity to the mass diffusivity of the inadequate reactant, is frequently used to characterize the instability of flames. It is generally accepted that when *Le* is greater than 1, diffusion contributes to flame stability; whereas when *Le* is less than 1, diffusion leads to flame instability.

We examine the influence of thermal diffusion on instability using the effective Lewis number (Le_{eff}) in order to better understand the cause of flame instability. Le_{eff} changes with equivalency ratio at various N_2 concentrations, as seen in Figure 6 (a). According to the findings, when the equivalency ratio is 0.8, Le_{eff} reaches its lowest value and remains below 1. Le_{eff} peaks at Φ = 1.0 and then progressively falls as the equivalency ratio rises, although it is always larger than 1. This suggests that a rich fuel mixture tends to maintain stability through thermal mass diffusion. Figure 6 (b) demonstrates how Le_{eff} changes for NH_3/N_2/syngas/air mixtures as a function of Φ under conditions where P_0 = 3 atm and T_u = 373 K. When the equivalency ratio rises, Leeff first rises until Φ = 1.0 and then falls once again. For both Φ = 0.8 and Φ = 1.4, Leeff remains less than one throughout this range of equivalence ratios. Furthermore, it was observed that increasing N_2 dilution content leads to a decrease in Leeff since under similar equivalence ratios, different N_2 concentrations result in gradually decreasing values for Leeff. The investigation of flame instability at various N_2 concentrations therefore suggests that thermal diffusive instability diminishes as N_2 concentration rises. The reason why the effective Lewis number is higher at equivalence ratio 1.0 but the flame is less stable than 1.2 and 1.4 can be attributed to a combination of factors: at high equivalence ratio, the increase in fuel concentration leads to a stronger exothermic reaction and a more stable flame propagation, and the higher fuel temperature and thermal diffusivity help maintain the flame stability. Excess fuel promotes favorable translation pathways and chain reactions. Thus, a more stable state of the flame appears in Figure 4.

ISSN: 2710-0588

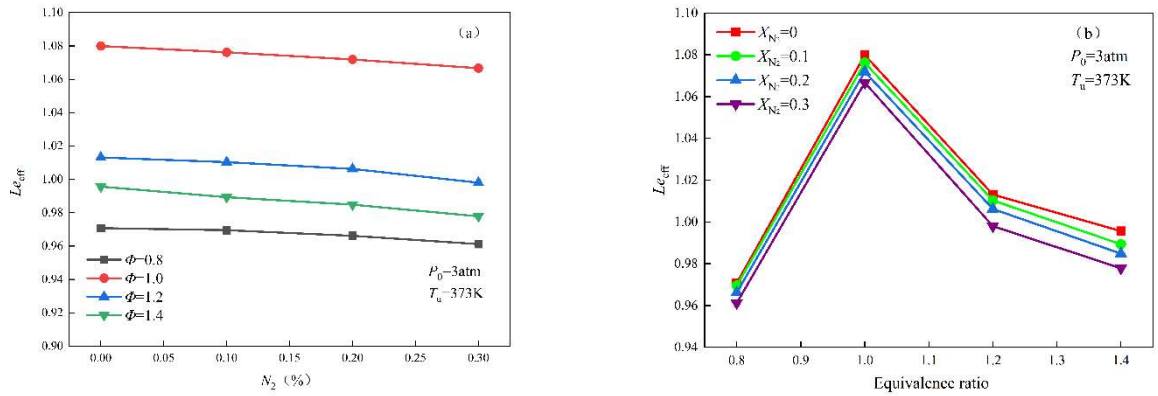

Figure 6. Leeff variation of NH_3/N_2/syngas/air mixture with N_2 concentration and equivalence ratio.

3.2.3. Hydrodynamic Instability

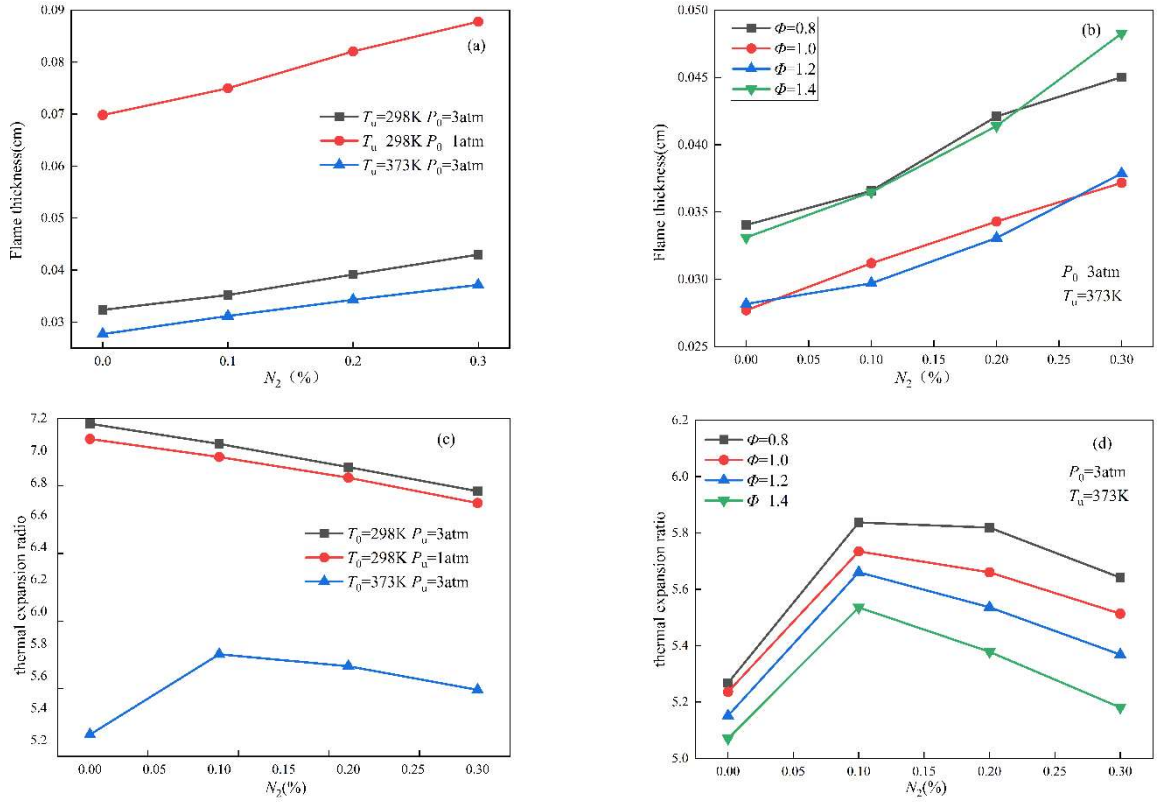

Figure 7. The variation of flame thickness and thermal expansion coefficient with the concentration of diluent N_2.

When a flame spreads across a larger area, hydrodynamic forces induce flame instability [42]. The hydrodynamic instability, which plays a crucial role in the dynamics of combustion, is influenced by two key parameters: the flame thickness, which determines the spatial scale over which chemical reactions occur, and the thermal expansion coefficient, which affects how the fluid's density changes with temperature and thus impacts the flow dynamics. Figure 7 (a) illustrates that both initial pressure and temperature impact the thickness of the flame. Specifically, higher initial temperatures result in smaller flame thicknesses, while higher initial pressures lead to reduced flame thicknesses. Furthermore, the impact of pressure on flame thickness is more pronounced compared to that of temperature. Under low pressure conditions, the flame exhibits a tendency towards increased thickness. Figure 7 (c) demonstrates that initial pressure and temperature also affect the coefficient of thermal expansion. Higher initial

ISSN: 2710-0588

temperatures correspond to smaller coefficients of thermal expansion. Conversely, larger initial pressures result in greater expansion coefficients; however, the effect of pressure on this coefficient is less pronounced compared to temperature variations. As initial temperatures increase, both the thermal expansion ratio and the flame thickness exhibit a decreasing trend. A more stable spherical flame expansion process is made possible by the reduced thermal expansion ratio on each side of the flame front. However, as the flame becomes thinner due to decreased thickness, it becomes more susceptible to baroclinic torque influences. Therefore, considering these interacting factors, it can be inferred that hydrodynamic instability may exhibit less sensitivity towards temperature.

Figure 7 (b) shows that the flame thickness progressively increases as the N_2 concentration rises. In the range of N_2 concentrations from 0 to 0.3, the flame thickness is greater than that under normal fuel conditions (Φ = 1.0) on both the fuel-lean side (Φ = 0.8) and the fuel-rich side (Φ = 1.2). Figure 7 (d) demonstrates that with an increase in N_2 concentration, the coefficient of thermal expansion initially rises, then slowly decreases, reaching a peak at a concentration of 0.1 N2. An increase in fuel volume causes the expansion coefficient to slightly decrease when the equivalency ratio changes; however, this change is minimal. Therefore, increasing N_2 concentration effectively inhibits hydrodynamic instability.

3.2.4. The Logarithmic Rate of Perturbation Growth

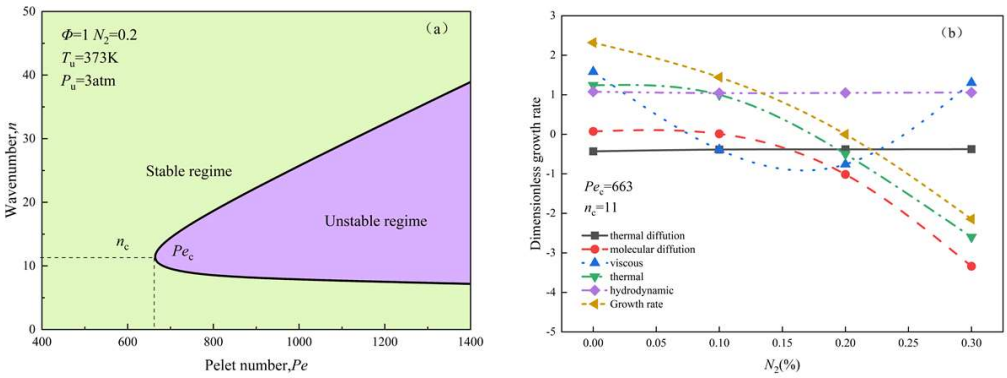

Figure 8. At Φ = 1.0, T_u = 373 K, the critical stability curve and logarithmic growth period of the premix flame in NH_3/N_2/syngas/air mixture (a) the critical stability curve and (b) the relationship between the growth rate and N_2 content.

The wave number and Peclet number (Pe) stability curves for the NH_3/N_2/syngas/air combination are shown in Figure 8 (a). The equation $\Sigma = 0$ defines the crucial stability curve, where $\Sigma < 0$ indicates a stable condition and $\Sigma > 0$ indicates an unstable state. As the flame advances, both the wave number and the number of cells on the flame surface rise. The flame is stable when Pe is less than Pe_c, but becomes unstable when Pe is more than Pe_c because of strong flame-stretching effects. Figure 8(b) illustrates the variation in the logarithmic growth rate of disturbances with changes in N_2 content under conditions of T_u = 373 K, Φ = 1.0, and P_0 = 3 atm. The logarithmic growth rate comprises hydrodynamic instability (ω) and diffusion instability ($-\Omega/Pe$) components. Thermal diffusion instability encompasses molecular diffusion ($-Ze(Le_{eff}-1)\ \Omega_2/(s-1)Pe$), thermal diffusion ($-\Omega_1/Pe$), and viscous diffusion ($-\Omega_3 Pr/Pe$). Disturbances with positive values indicate a stable flame state, while negative values represent an unstable state. All data presented in Figure 8(b) were obtained under nc = 11 conditions with Pe_c = 663 [44]. Thermal diffusion, molecular diffusion, and viscous diffusion all exert

ISSN: 2710-0588

significant effects on diffusion-thermal instability. The instability is mainly affected by diffusion-thermal instability, among which molecular diffusion instability and thermal diffusion instability have the greatest influence. Hydrodynamic instability remains consistently positive and exhibits minimal variation with changes in N_2 concentration. This results in the flame instability of the mixed fuel (∑) gradually decreasing as the N_2 concentration increases, becoming negative when N_2 > 0.2. These observations indicate that overall flame stability improves with increasing N_2 concentration, the flame gradually changed from wrinkled to smooth, which aligns with the analysis presented in Figure 5.

3.3. Chemical Kinetics Analysis

3.3.1. Sensitivity Analysis

Figure 9 illustrates the fluctuation in the normalized sensitivity coefficient of LBV for NH_3/N_2/syngas/air mixture under circumstances of Φ = 0.8, 1.0, 1.2, and 1.4 at P_0 = 3 atm and Tu = 373 K in order to examine the impact of diluent N_2 on the LBV. The sensitivity coefficient is represented by the horizontal axis; positive and negative values show that the initial reaction rate had both promoting and inhibitory impacts on LBV [43].

As depicted in Figure 9, a main reaction steps significantly influence the LBV of the mixture: H_2/O_2 reaction. Among these reactions, the chain-branching reaction R39: H + O_2 → O + OH demonstrates the highest sensitivity coefficient. In conjunction with reactions R85 and R102, this process generates a significant quantity of H radicals that positively affect LBV. Conversely, reaction R36 exhibits a pronounced negative sensitivity due to its role in reducing fuel reactivity through the production of reactive HO_2 radicals, an effect that is particularly evident at low equivalence ratios.

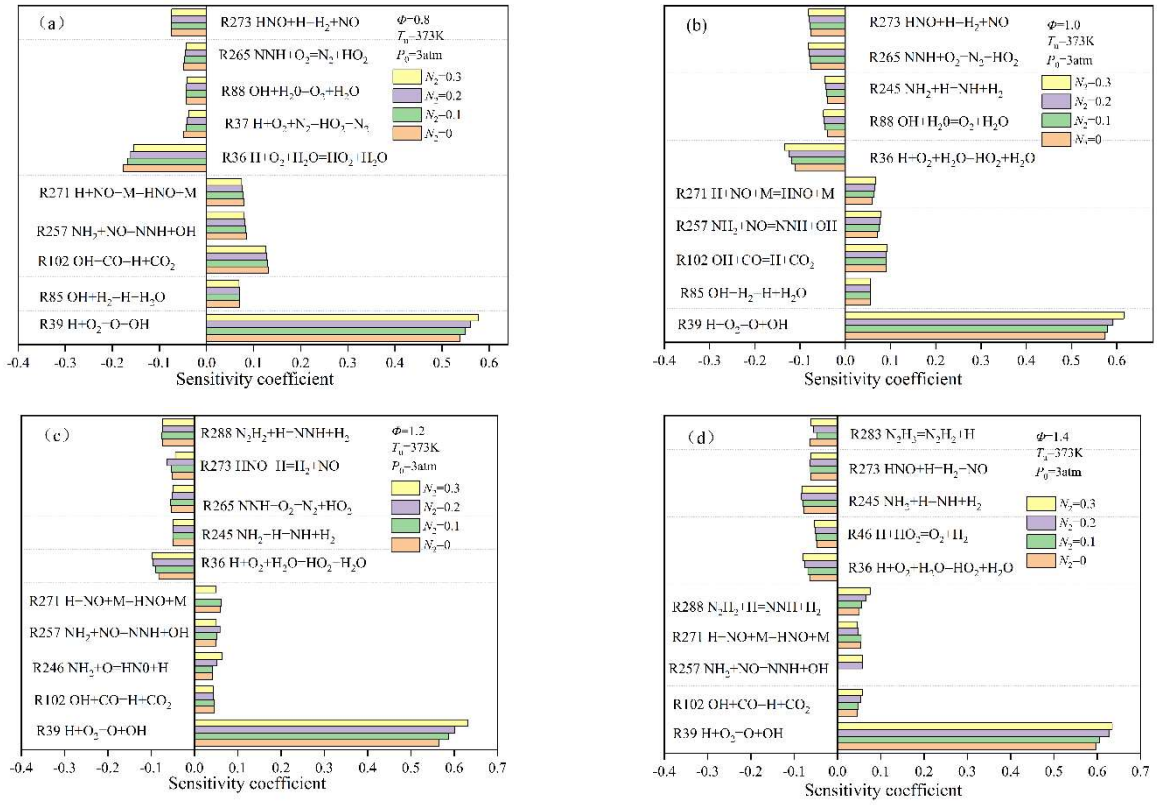

Figure 9. Sensitivity analysis of different N_2 concentrations of NH_3/N_2/syngas/air mixtures at P_0 = 3 atm, T_u = 373 K.

The figure demonstrates that part radical reactions' absolute value of sensitivity coefficients increases with N_2 dilution under different equivalence ratios. This phenomenon can be

ISSN: 2710-0588

attributed to temperature's influence on reaction rates; adding diluent decreases flame temperature, thereby slowing down reactions and enhancing free radical reactions' rate-limiting effect. Overall results indicate that the rate-limiting effect caused by original reactions is enhanced by the addition of diluent.

3.3.2. Impact of Diluent N2 on Intermediate Species

Different radical pools will affect the oxidation process of fuel and the formation of NO_x. Figure 10. analyzes the influence of the N_2 dilution on radicals and key intermediate products, highlighting difference in the concentration of the primary product and critical intermediate radical at Φ = 1.0 and 1.4 and N_2 concentrations of 0 and 0.3. The concentrations of intermediates and radicals drop in tandem with a decrease in the reactant concentration. Figure 10. (a) and (c) illustrates that the concentrations of O, OH, and NO radicals in the radical pool are elevated under low fuel conditions. This occurrence is due to an insufficient fuel supply, which encourages the further oxidation of intermediate H_2, leading in the creation of OH radicals and the synthesis of end products. According to Figure 10. (b) and (d), under fuel-rich conditions, NH_3 decomposed to form more NH_2 radicals and N_2H_3 products, which influenced the formation of NO. In general, the addition of N_2 thinner can effectively reduce the generation of NO pollutants.

Figure 11 illustrates the net reaction rate of the mixture under two conditions: diluent N_2 = 0 and 0.3. Notably, R39 and R102 exhibited higher net reaction rates compared to other reactions. Additionally, the net reaction rate of NH_3 decomposition branch chain reactions R271 and R257 was also significant. The elevated net reaction rate of R39 primarily resulted from the substantial consumption of OH radicals, which facilitated the production of H radicals. As the content of diluent N_2 increased, there was a substantial decrease in the net branched chain reaction rate, leading to a decline in peak value for maximum reaction rate from 0.023 mole/cm^3/s to 0.011 mole/cm^3/s.

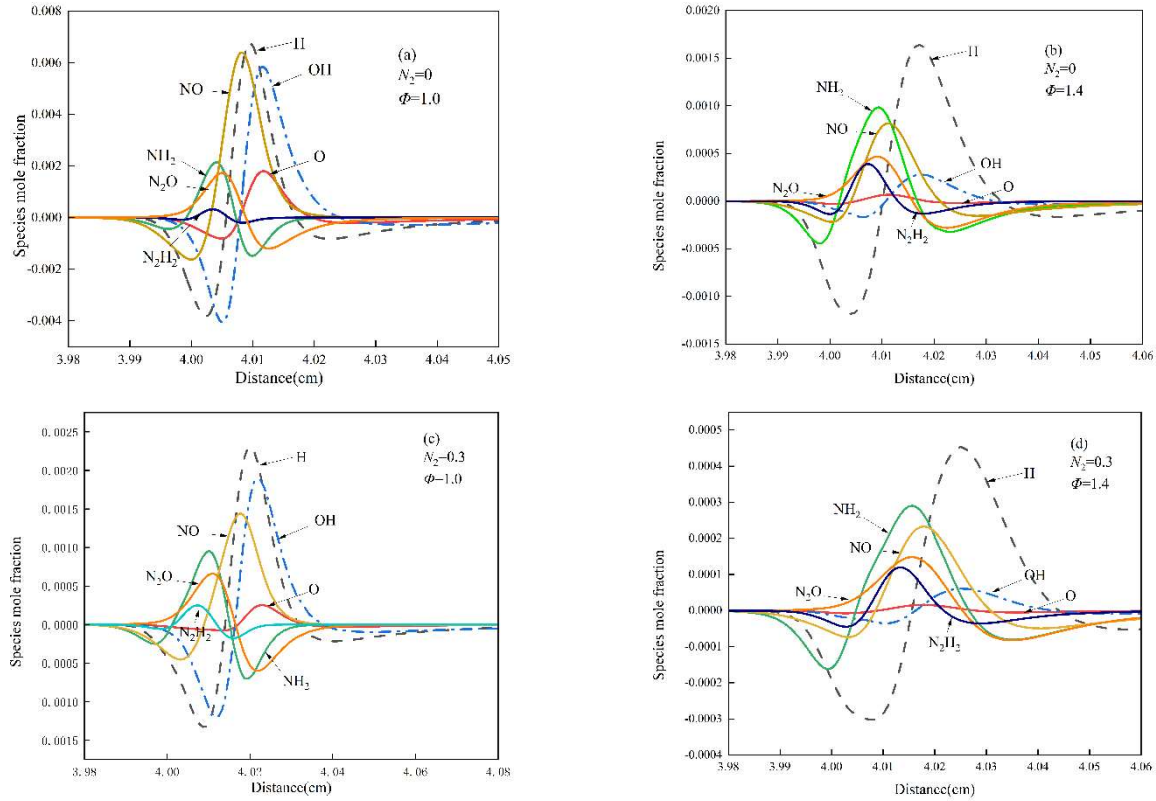

Figure 10. Key intermediate species of N_1 and N_{400} mixtures.

ISSN: 2710-0588

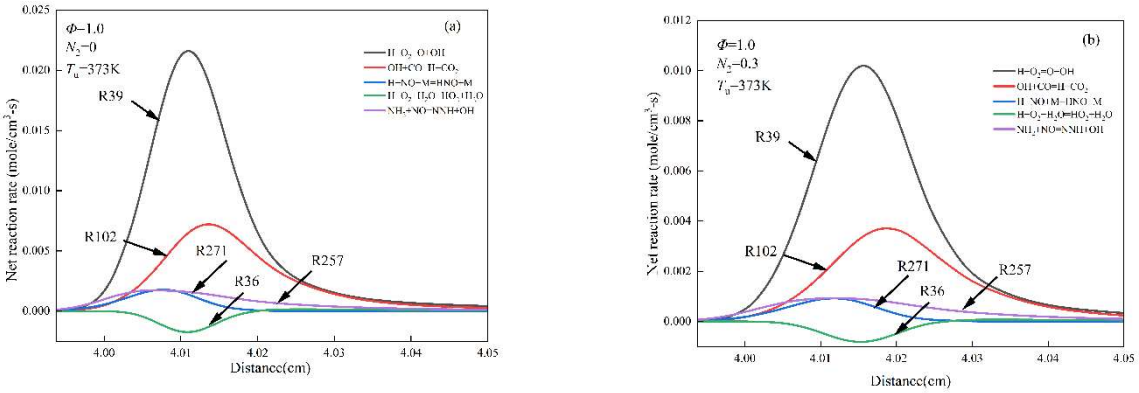

Figure 11. Net reaction rate of NH_3/N_2/syngas/air mixtures with N_2 = 0 and 0.3(Φ = 1.0, T_u = 373 K).

4. Conclusion

The effects of the equivalence ratio (Φ = 0.8-1.4), starting temperature (T_u = 298 K, 373 K), initial pressure (P_0 = 1 atm, 3 atm), and diluent nitrogen (X = 0-0.3) on the LBV and flame instability of NH_3/syngas/air flames were investigated in detail using the spherical flame propagation technique. Combustion of NH_3/syngas/air flame mixtures has enormous industrial potential. The quick overview is summarized as follows.

(1) The LBV of the NH_3/N_2/syngas/air combination swings non-monotonically with respect to the equivalency ratio (Φ), increasing first and then reducing as Φ increases. The peak LBV value is observed at Φ = 1.1, and this peak equivalence ratio shifts towards higher values with an increase in diluent N_2 concentration, and LBV shows a significant enhancement with rising temperature.

(2) Through the analysis of flame instability, it has been observed that the Leeff (effective Lewis number) of NH_3/N_2/syngas/air mixture flame is not significantly influenced by the concentration of diluent N_2. Furthermore, the variation in the equivalence ratio does not display a monotonic trend; in contrast, it first rises and then falls as the value of Φ grows. Temperature is found to have a significant impact on hydrodynamic instability, with an increase in starting temperature suppressing the onset of hydrodynamic instability.

(3) The thermal diffusivity of the NH_3/syngas/air flame initially intensifies and subsequently diminishes as diluent N_2 is added. This phenomenon is mainly due to the interaction between the concentration of reactive components and the specific heat capacity of the mixture. In lean mixtures, diffusion thermal instability is observed, while stability is achieved in rich mixtures.

(4) The logarithmic growth rate of disturbances diminishes as diluent N_2 content increases, indicating a reduction in flame instability.

For NH_3/N_2/syngas/air mixture, the main reaction that affects LBV is that $H+O_2=O+OH$, $OH+H_2=H+H_2O$, $OH+CO=H+CO_2$, which positively influences LBV. Diluent N_2 strengthens the reaction's rate-limiting impact while preventing the production of H/OH free radicals.

Acknowledgments

This work was supported by the National Natural Science Foundation of China [No.52004085].

References

[1] Kobayashi H, Hayakawa A, Somarathne KKA, Okafor EC. Science and technology of ammonia combustion. Proc Combust Inst 2019;37(1):109-33. https://doi.org/10.1016/j.proci.2018.09.029.

ISSN: 2710-0588

[2] Cardoso JS, Silva V, Rocha RC, Hall MJ, Costa M, Eusébio D. Ammonia as an energy vector: current and future prospects for low-carbon fuel applications in internal combustion engines. J Clean Prod 2021;296:126562. https://doi.org/10.1016/j.jclepro.2021.126562.

[3] Hayakawa A, Goto T, Mimoto R, Arakawa Y, Kudo T, Kobayashi H. Laminar burning velocity and markstein length of ammonia/air premixed flames at various pressures. Fuel (Lond) 2015;159:98-106. https://doi.org/10.1016/j.fuel.2015.06.070.

[4] Ma F, Guo L, Li Z, Zeng X, Zheng Z, Li W, et al. A review of current advances in ammonia combustion from the fundamentals to applications in internal combustion engines. Energies 2023;16(17):6304. https://doi.org/10.3390/en16176304.

[5] Ziyaei S, Mazlan SK, Lappas P. A review of ultra-lean and stratified charged combustion in natural gas spark ignition engines. Sae Int J Engines 2023;16(03-16-07-0050):883-922. https://doi.org/10.4271/03-16-07-0050.

[6] Singh AS, Dash SK, Reddy VM. Chemical kinetic analysis on influence of hydrogen enrichment on the combustion characteristics of ammonia air using newly proposed reaction model. Int J Energy Res 2022;46(5):6144-63. https://doi.org/10.1002/er.7554

[7] Mashruk S, Shi H, Mazzotta L, Ustun CE, Aravind B, Meloni R, et al. Perspectives on no x emissions and impacts from ammonia combustion processes. Energy Fuels 2024;38(20):19253-92. https://doi.org/10.1021/acs.energyfuels.4c03381.

[8] Lhuillier C, Brequigny P, Lamoureux N, Contino F, Mounaïm-Rousselle C. Experimental investigation on laminar burning velocities of ammonia/hydrogen/air mixtures at elevated temperatures. Fuel (Lond) 2020;263:116653. https://doi.org/10.1016/j.fuel.2019.116653.

[9] Wang Z, Yu Z, Chen C, He Y, Zhu Y. Research progress on combustion characteristics of new zero carbon ammonia fuel. J. Huazhong Univ. Sci. Technol.(Nat. Sci. Ed.) 2022;50:27-40. https://doi.org/10.13245/j.hust.220703.

[10] Li J, Lai S, Chen D, Wu R, Kobayashi N, Deng L, et al. A review on combustion characteristics of ammonia as a carbon-free fuel. Front Energy Res 2021;9:760356. https://doi.org/10.3389/fenrg.2021.760356.

[11] Lee JH, Lee SI, Kwon OC. Effects of ammonia substitution on hydrogen/air flame propagation and emissions. Int J Hydrogen Energy 2010;35(20):11332-41. https://doi.org/10.1016/j.ijhydene.2010.07.104.

[12] Chen J, Chen G, Zhang A, Deng H, Wen X, Wang F, et al. Experimental and numerical study on the effect of co2 dilution on the laminar combustion characteristics of premixed ch4/h2/air flame. J Energy Inst 2022;102:315-26. https://doi.org/10.1016/j.joei.2022.04.002.

[13] Chu H, Xiang L, Meng S, Dong W, Gu M, Li Z. Effects of n2 dilution on laminar burning velocity, combustion characteristics and nox emissions of rich ch4–air premixed flames. Fuel (Lond) 2021;284:119017. https://doi.org/10.1016/j.fuel.2020.119017.

[14] Han X, Wang Z, Costa M, Sun Z, He Y, Cen K. Experimental and kinetic modeling study of laminar burning velocities of nh3/air, nh3/h2/air, nh3/co/air and nh3/ch4/air premixed flames. Combust Flame 2019;206:214-26. https://doi.org/10.1016/j.combustflame.2019.05.003.

[15] Wang S, Wang Z, Elbaz AM, Han X, He Y, Costa M, et al. Experimental study and kinetic analysis of the laminar burning velocity of nh3/syngas/air, nh3/co/air and nh3/h2/air premixed flames at elevated pressures. Combust Flame 2020;221:270-87. https://doi.org/10.1016/j.combustflame.2020.08.004.

[16] Lee JH, Kim JH, Park JH, Kwon OC. Studies on properties of laminar premixed hydrogen-added ammonia/air flames for hydrogen production. Int J Hydrogen Energy 2010;35(3):1054-64. https://doi.org/10.1016/j.ijhydene.2009.11.071.

[17] Mousavi SM, Lee BJ, Kim J, Sotoudeh F, Chun B, Jun D, et al. On the effects of adding syngas to an ammonia-mild combustion regime-a computational study of the reaction zone structure. Int J Hydrogen Energy 2024;52:226-40. https://doi.org/10.1016/j.ijhydene.2023.03.441.

[18] Mousavi SM, Sotoudeh F, Jun D, Lee BJ, Esfahani JA, Karimi N. On the effects of nh3 addition to a reacting mixture of h2/ch4 under mild combustion regime: numerical modeling with a modified

ISSN: 2710-0588

edc combustion model. Fuel (Lond) 2022;326:125096. https://doi.org/10.1016/j.fuel.2022.125096.

[19] Kiani M, Kohansal M, Masoumi S, Ashjaee M, Houshfar E. An experimental investigation on non-preheated mild combustion of syngas/ammonia/air. J Therm Anal Calorim 2023;148(21):11783-97. https://doi.org/10.1007/s10973-023-12512-7.

[20] Mei B, Ma S, Zhang Y, Zhang X, Li W, Li Y. Exploration on laminar flame propagation of ammonia and syngas mixtures up to 10 atm. Combust Flame 2020;220:368-77. https://doi.org/10.1016/j.combustflame.2020.07.011.

[21] Mei B, Zhang J, Shi X, Xi Z, Li Y. Enhancement of ammonia combustion with partial fuel cracking strategy: laminar flame propagation and kinetic modeling investigation of nh3/h2/n2/air mixtures up to 10 atm. Combust Flame 2021;231:111472. https://doi.org/10.1016/j.combustflame.2021.111472.

[22] Askari O, Moghaddas A, Alholm A, Vien K, Alhazmi B, Metghalchi H. Laminar burning speed measurement and flame instability study of h2/co/air mixtures at high temperatures and pressures using a novel multi-shell model. Combust Flame 2016;168:20-31. https://doi.org/10.1016/j.combustflame.2016.03.018.

[23] Kelley AP, Law CK. Nonlinear effects in the extraction of laminar flame speeds from expanding spherical flames. Combust Flame 2009;156(9):1844-51. https://doi.org/10.1016/j.combustflame.2009.04.004.

[24] Burke MP, Chen Z, Ju Y, Dryer FL. Effect of cylindrical confinement on the determination of laminar flame speeds using outwardly propagating flames. Combust Flame 2009;156(4):771-9. https://doi.org/10.1016/j.combustflame.2009.01.013.

[25] Bradley D, Hicks RA, Lawes M, Sheppard CGW, Woolley R. The measurement of laminar burning velocities and markstein numbers for iso-octane–air and iso-octane–n-heptane–air mixtures at elevated temperatures and pressures in an explosion bomb. Combust Flame 1998;115(1):126-44. https://doi.org/10.1016/S0010-2180(97)00349-0.

[26] Bradley D, Harper CM. The development of instabilities in laminar explosion flames. Combust Flame 1994;99(3):562-72. https://doi.org/10.1016/0010-2180(94)90049-3.

[27] Burke MP, Chen Z, Ju Y, Dryer FL. Effect of cylindrical confinement on the determination of laminar flame speeds using outwardly propagating flames. Combust Flame 2009;156(4):771-9. https://doi.org/10.1016/j.combustflame.2009.01.013.

[28] Bray K. Turbulent combustion. By norbert peters. Cambridge university press, 2000. 320 pp. Isbn 0521 60823. $45. J Fluid Mech 2001;426:407-9. https://doi.org/10.1017/S0022112000002676.

[29] Davis SG, Quinard J, Searby G. Markstein numbers in counterflow, methane-and propane-air flames: a computational study. Combust Flame 2002;130(1-2):123-36. https://doi.org/10.1016/S0010-2180(02)00368-1.

[30] Clavin P. Dynamic behavior of premixed flame fronts in laminar and turbulent flows. Prog Energy Combust Sci 1985;11(1):1-59. https://doi.org/10.1016/0360-1285(85)90012-7.

[31] Egolfopoulos FN, Hansen N, Ju Y, Kohse-Höinghaus K, Law CK, Qi F. Advances and challenges in laminar flame experiments and implications for combustion chemistry. Prog Energy Combust Sci 2014;43:36-67. https://doi.org/10.1016/j.pecs.2014.04.004.

[32] Law CK, Sung CJ. Structure, aerodynamics, and geometry of premixed flamelets. Prog Energy Combust Sci 2000;26(4-6):459-505. https://doi.org/10.1016/S0360-1285(00)00018-6.

[33] Chung K. Law. Combustion physics. New York 2006.https://doi.org/10.1016/j.proci.2006.08.124.

[34] Prathap C, Ray A, Ravi MR. Investigation of nitrogen dilution effects on the laminar burning velocity and flame stability of syngas fuel at atmospheric condition. Combust Flame 2008;155(1):145-60. https://doi.org/10.1016/j.combustflame.2008.04.005.

[35] Poinsot T. Prediction and control of combustion instabilities in real engines. Proc Combust Inst 2017;36(1):1-28. https://doi.org/10.1016/j.proci.2016.05.007.

ISSN: 2710-0588

[36] Li T, Wang XR, Ma Y, Wang L, Oppong F, Xu C, et al. Investigation on hydrogen/ethanol intrinsic flame instability. Combust Flame 2022;241:112064. https://doi.org/10.1016/j.combustflame.2022.112064.

[37] Addabbo R, Bechtold JK, Matalon M. Wrinkling of spherically expanding flames. Proc Combust Inst 2002;29(2):1527-35. https://doi.org/10.1016/S1540-7489(02)80187-0.

[38] Kobayashi H, Hayakawa A, Somarathne KDKA, Okafor EC. Science and technology of ammonia combustion. Proc Combust Inst 2019;37(1):109-33. https://doi.org/10.1016/j.proci.2018.09.029.

[39] Zhou C, Li Y, Burke U, Banyon C, Somers KP, Ding S, et al. An experimental and chemical kinetic modeling study of 1,3-butadiene combustion: ignition delay time and laminar flame speed measurements. Combust Flame 2018;197:423-38. https://doi.org/10.1016/j.combustflame.2018.08.006.

[40] Reddy H, Abraham J. A numerical study of vortex interactions with flames developing from ignition kernels in lean methane/air mixtures. Combust Flame 2011;158(3):401-15. https://doi.org/10.1016/j.combustflame.2010.09.008.

[41] Mei B, Ma S, Zhang Y, Zhang X, Li W, Li Y. Exploration on laminar flame propagation of ammonia and syngas mixtures up to 10 atm. Combust Flame 2020;220:368-77. https://doi.org/10.1016/j.combustflame.2020.07.011.

[42] Han X, Wang Z, Costa M, Sun Z, He Y, Cen K. Experimental and kinetic modeling study of laminar burning velocities of nh3/air, nh3/h2/air, nh3/co/air and nh3/ch4/air premixed flames. Combust Flame 2019;206:214-26. https://doi.org/10.1016/j.combustflame.2019.05.003.

[43] Matalon M. Flame dynamics. Proc Combust Inst 2009;32(1):57-82. https://doi.org/10.1016/j.proci.2008.08.002

[44] Mack LM. Boundary-layer linear stability theory. Agard Rep 1984;709. https://doi.org/10.4271/1984-01-1410.